HHS Public Access

Author manuscript

Mol Pharm. Author manuscript; available in PMC 2016 September 08.

Published in final edited form as:

Mol Pharm. 2015 September 8; 12(9): 3250–3260. doi:10.1021/acs.molpharmaceut.5b00216.

Dual Receptor-Targeted Theranostic Nanoparticles for Localized Delivery and Activation of Photodynamic Therapy Drug in Glioblastomas

Suraj Dixit[†], **Kayla Miller**[†], **Yun Zhu**[†], **Emilie McKinnon**[‡], **Thomas Novak**[†], **Malcolm E. Kenney**[⊥], and **Ann-Marie Broome**[*,†,‡,§]

[†]Department of Radiology and Radiological Sciences, Medical University of South Carolina, Charleston, South Carolina 29425, United States

[‡]Center of Biomedical Imaging, Medical University of South Carolina, Charleston, South Carolina 29425, United States

[§]Department of Neurosciences, Medical University of South Carolina, Charleston, South Carolina 29425, United States

[⊥]Department of Chemistry, Case Western Reserve University, Cleveland, Ohio 44106, United States

Abstract

Targeting gold nanoparticles (AuNPs) with two or more receptor binding peptides has been proposed to address intratumoral heterogeneity of glioblastomas that overexpress multiple cell surface receptors to ultimately improve therapeutic efficacy. AuNPs conjugated with peptides against both the epidermal growth factor and transferrin receptors and loaded with the photosensitizer phthalocyanine 4 (Pc 4) have been designed and compared with monotargeted AuNPs for *in vitro* and *in vivo* studies. The (EGF_{pep}+Tf_{pep})-AuNPs-Pc 4 with a particle size of ~41 nm improved both specificity and worked synergistically to decrease time of maximal accumulation in human glioma cells that overexpressed two cell surface receptors as compared to cells that overexpressed only one. Enhanced cellular association and increased cytotoxicity were achieved. *In vivo* studies show notable accumulation of these agents in the brain tumor regions.

[*]**Corresponding Author**: broomea@musc.edu. Phone: 1-843-876-2481. Fax: 1-843-876-2469..

ASSOCIATED CONTENT

Supporting Information

The Supporting Information is available free of charge on the ACS Publications website at DOI: 10.1021/acs.molpharmaceut.5b00216.

Electrophoretic mobility of negatively charged AuNPs in an agarose gel and associated Pc 4 fluorescence; EGFR and TfR overexpression in glioma cells, including Western blot and immunofluorescence localization of the receptors (PDF)

Author Contributions

The manuscript was written through contributions of all authors. All authors have given approval to the final version of the manuscript.

The authors declare no competing financial interest.

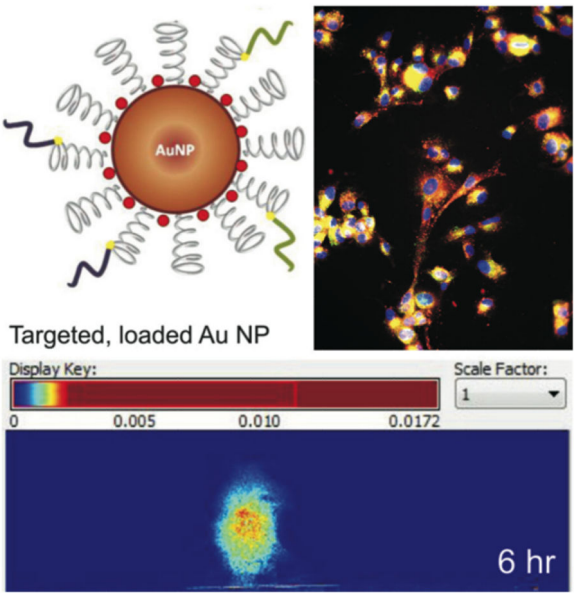

Keywords

gold nanoparticles; epidermal growth factor; transferrin; Pc 4; glioblastoma

INTRODUCTION

Brain tumors (gliomas) are among the most deadly tumor subtypes because tumor location, grade, histopathology, and recurrence play critical roles in the patient's survival rate. Despite recent advances in the treatment of gliomas, Glioblastoma Multiform (GBM, primary high grade malignant brain tumor) remains the most difficult to treat of the glioma subtypes, and little progress has been achieved in prolonging the dismal patient survival rates of less than 12 months after diagnosis.[1,2] Currently, detection of GBMs relies on targeting single biomarkers in a heterogeneous environment. Chemotherapeutics for GBM suffer from a major drawback, lack of tumor selectivity, which causes significant collateral cell death in healthy cells.[3] Further, GBM tumors are separated from the rest of the body by the blood brain barrier (BBB). The BBB poses a physical obstacle for drug delivery, resulting in low drug bioavailability.[4] Lately, nanoparticles with more ideal physiological properties, such as small size, increased stability, and improved biocompatibility, have revealed the potential of novel nanocarriers in GBM research and therapies.[5–7] The main advantages of these nanoparticles lie in the ability of scientists to tailor their surface with tumor specific targeting moieties and to deliver hydrophobic anticancer drugs without affecting drug activity.[8,9]

In the past, solid-core nanoparticles (iron oxide,[10,11] gadolinium oxide,[12,13] or manganese oxide[14,15]) have been utilized to detect brain gliomas and deliver drugs. However, these nanoparticles cause severe cytotoxicity due to degradation byproducts and leaching of toxic metal ions.[16] Other nanoparticles, such as quantum dots (QDs), face similar degradation problems affecting their biocompatibility.[17,18] This necessitates targeted, biocompatible

nanoparticles for long-term imaging and chemotherapy. In this capacity, gold nanoparticles (AuNPs) fit the goals of efficient drug delivery since they have low cytotoxicity (as they are more inert and resistant to degradation), tunable sizes, and excellent surface chemistries for firm conjugation of ligands.[19,20]

Polyethylene glycol (PEG)-coated AuNPs have been used for drug delivery in cancer cells.[19,21–23] PEGylation serves two functions: reduction of nonspecific interactions with the PEG molecule to allow longer circulation times in the bloodstream and creation of an amphiphilic corona of PEG molecules to encapsulate hydrophilic biomolecules.[19,22] Additionally, functional moieties on the PEG can be used to conjugate specific ligands for targeting cancer biomarkers overexpressed by tumor cells thereby conferring active targeting capabilities to the nanoparticles.[24]

Intraoperative photodynamic therapy (PDT) represents a shift in tumor treatment regimes away from more conventional resection followed by systemic chemotherapeutics. PDT is being developed as an adjuvant to tumor resection, but has thus far failed in clinical trials for various reasons.[25,26] One of the identifiable shortcomings of PDT for the treatment of GBMs, which is based on light-mediated activation of a photosensitizer, is the systemic delivery of the photosensitizer to healthy tissues in addition to the cancerous tissue. During PDT, even if the light activation beam is focused to a relatively small region, the systemically delivered photosensitizer can rapidly induce nontargeted phototoxicity within the surrounding tissue and cells.[27,28]

To overcome issues of nonspecific photosensitizer accumulation, studies have been performed with AuNPs targeted to single biomarkers.[24,29] For instance, previous work completed in our laboratory showed that epidermal growth factor receptor (EGFR)-targeted AuNPs loaded with the photosensitizer Pc 4 showed reduced systemic cytotoxicity and increased drug delivery efficiency as compared to untargeted AuNPs.[24] This strategy can be improved by increasing the selectivity of the AuNPs since glioma cells overexpress multiple biomarkers in a heterogeneous manner.[30] Heterogeneity contributes to the GBM's aggressiveness and poses a significant obstacle to the design of effective therapies. In fact, minor tumor cell populations within a heterogeneous mass have been found to potently accelerate growth and could provide novel targets of therapeutic intervention.[31] The rationale of our current work is to design a multifunctional AuNP with two targeting moieties loaded onto AuNPs adsorbed with Pc 4 to increase both the selectivity and specificity of drug delivery as compared to monotargeted AuNPs.

In this study, a dual-targeted AuNP system consisting of epidermal growth factor (EGF_{pep}) and transferrin (Tf_{pep}) peptides loaded with Pc 4 is designed and tested for cellular uptake and cytotoxic drug efficacy. Both EGF and Tf receptors (EGFR and TfR, respectively) are overexpressed in brain tumors at varying levels. Dual-targeted AuNPs show drastic improvement in drug uptake and cell killing as compared to monotargeted AuNPs due to the synergistic endocytosis mechanism of the ligands on the same drug delivery agent. In addition, dual-targeted AuNPs show increased accumulation of drug in orthotopic tumor regions of implanted mice in contrast to monotargeted AuNPs.

EXPERIMENTAL SECTION

Synthesis of PEGylated AuNPs

Hydrophobic tetraoctyl-ammonium bromide (TOAB)-coated AuNPs were synthesized via modified Brust–Schiffrin method.[24,32,33] Typically, 0.1367 g of TOAB was added to 5 mL of toluene followed by addition of 367 μL of 30 wt % of Gold(III) chloride solution. The solution was stirred at room temperature for 5 min. To this solution, 0.112 g of DDA (dodecylamine) was added and stirred at room temperature for 10 min. A solution of 0.0756 g of sodium borohydride ($NaBH_4$) was made in 1 mL of ice-cold nanopure water in a separate tube. This $NaBH_4$ solution was added slowly to the gold chloride salt solution. The resulting reaction mixture was stirred at room temperature for 2 h. For purification, the entire reaction mixture was poured in 50 mL of ethanol to precipitate the AuNPs. The AuNPs were centrifuged at 6000 rpm for 15 min and the supernatant discarded. This process was repeated three times to remove any excess surfactants. The particles were dried under nitrogen for 30 min. For PEGylation, the particles were dissolved in 5 mL of chloroform, and 1000-fold excess of monofunctional PEG (SH-PEG-methoxy, 5 kDa) and bifunctional PEG (SH-PEG-COOH, 5 kDa) at a final ratio of (4:1) in 200 μL of chloroform was added to AuNPs solution in chloroform. The mixture was stirred at room temperature for 2 days and then air-dried. The resulting pellet was dissolved in nanopure water followed by three washes using 10K MWCO ultracentrifugal filter (EMD Millipore, MA) at 4000 rpm for 15 min at room temperature. This was done to ensure removal of excess thiolated PEG reagents.

Peptide Conjugation of AuNPs

PEGylated AuNPs were conjugated to EGF_{pep} and Tf_{pep} peptides (1:10 molar ratio of carboxyl groups on AuNPs to peptide) using the EDC/NHS protocol via the formation of covalent amide bond. Typically, Sulfo-NHS and EDC (10 mg per 100 μL of MES buffer, pH 4.5) were added to PEGylated AuNPs in 1 mL of MES buffer and stirred for 15 min at room temperature. After incubation, the pH of the solution was raised to 7.5 by adding PBS buffer (pH ≈ 12). EGF_{pep} (10 μL, 1 mg per 200 μL of DMSO) and 5 μL of Tf_{pep} (1 mg per 200 μL of DMSO) were added to this solution for peptide conjugation followed by stirring at room temperature for 2 h. The excess reagents (peptides, EDC, NHS) were removed using a 10K MWCO ultracentrifugal centrifugation device (EMD Millipore, MA) at 4000 rpm for 15 min. This purification was repeated three times using nanopure water.

Pc 4 Loading on AuNPs

Targeted AuNPs or untargeted AuNPs in nanopure water were vacuum-dried and resuspended in chloroform. Pc 4 was added to the reaction solution at a ratio of 40:1 (Pc 4 molecules to AuNPs). The reaction solution was stirred at room temperature and protected from light for 2 days. After the incubation, chloroform was evaporated, resuspended in nanopure water, and sonicated for 2 h at room temperature. Excess Pc 4 was removed by purification with 10K MWCO ultracentrifugal device at 4000 rpm at 4 °C.

Size and Concentration Characterization of AuNPs

The concentrations of AuNPs, PEGylated AuNPs, (EGF_{pep}+Tf_{pep})-AuNPs, and Pc 4-loaded AuNPs were determined by UV–vis absorption using a Biotek plate reader (Biotek, VT). Transmission electron microscopy (TEM) micrographs of AuNPs were taken by spreading organic and aqueous master solution (1 mg mL^{-1}) on a carbon-coated copper grid. The excess solution was removed, followed by air-drying. The sample was visualized with a transmission electron microscope equipped with a digital camera (JEOL, MA) at 80 kV. Dynamic Light Scattering (DLS) and zeta potential of AuNPs preparations in aqueous solution were performed on a ZetaPals particle analyzer (Brookhaven Instruments, NY). To prepare DLS samples, the respective organic and aqueous master solution (1 mg mL^{-1}) was diluted five-fold and sonicated to prevent aggregation. The solution was subsequently filtered using a 0.2 μm syringe filter before the measurements were taken.

Gel electrophoresis was used for determination of the anionic functional group attachment and Pc 4 attachment to the AuNPs preparations. Samples were run at 90 V, and the mobility of the sample was determined by measuring the relative displacements with a CCD-equipped stereomicroscope. Pc 4 fluorescence was observed at 670 nm on a Maestro small animal imager (PerkinElmer, MA).

NP stability and drug release of Pc 4 from untargeted AuNPs or targeted AuNPs were analyzed via UV–vis spectroscopy. The samples (5 μL) were mixed with 200 μL of PBS buffer (pH 7.4, 0.01 M) in a 96-well plate to a final concentration of 1 mM. UV–vis measurements were taken every hour for a total of 24 h at 630 nm (Pc 4) and 505 nm (AuNPs) using Biotek plate reader (Biotek, VT) at room temperature.

CELL CULTURE

Human glioblastoma astrocytoma, epithelial-like cell lines, U87-MG and LN229 were used in these studies. U87-MG and LN229 cells were obtained from American Type Culture Collection. Cell lines were maintained in Dulbecco's Modified Eagle's Medium (cDMEM; Gibco) and supplemented with 10% FBS and 1% penicillin–streptomycin. The cells were incubated at 37 °C in a humidified 5% CO_2 atmosphere.

In Vitro AuNP Uptake Assays

Glioma cell lines, LN229 and U87, were plated on a 25 × 25 mm^2 coverslips at a density of 30 000 cells per slip and maintained in cDMEM at 37 °C in an incubator supplied with 5% CO_2. Cells were treated with various concentrations of Pc 4-loaded AuNPs for 1, 4, 8, or 24 h. Immunostaining was done to observe the colocalization of the drug, AuNPs, and receptors. After incubation, the cells were fixed with 4% paraformaldehyde followed by washing with PBS buffer. Nuclei were stained with 4′,6-diamidino-2-phenylindole (DAPI). The uptake and colocalization was visualized by fluorescence microscope using a Leica DM 4000B microscope (Leica Microsystems, IL). Quantitative analyses for colocalization studies were performed employing Leica LAS-AF image analysis, where a region of interest (ROI) was manually selected, and measurements of relative mean intensity of the fluorescence images were overlaid to reveal colocalized pixels.

Colocalization Immunofluorescence

Human glioma cells were plated at a density of 30 000 cells per coverslip and treated with 500 nM Au-NPs-Pc 4 or (EGF_{pep}+Tf_{pep})-Au-NPs-Pc 4 for 0, 5, 15, 30, and 60 min. The cells were concomitantly incubated with EGF-Alexa 555 (E35350; 100 nM; Invitrogen, NY) to identify EGF endosomes and Tf-Alexa 488 (T13342; 250 nM; Invitrogen, NY) to identify Tf endosomes in a final volume of 250 μL of cell media. The cells were washed with media and fixed with 4% paraformaldehyde. The stained, fixed cells were counter-stained with DAPI nuclear stain. In another experiment, glioma cells (30 000 per coverslip) were treated with 500 nM (EGF_{pep}+Tf_{pep})-Au-NPs-Pc 4 for 4 h, fixed with 4% paraformaldehyde, blocked with 3% goat serum for 1 h and immunostained with anti-LAMP2 (L0668; 1:500; Sigma-Aldrich, MO) for lysosomes for 1 h, washed with PBS buffer, followed by staining with secondary antigoat Alexa 488 (1:1000; Invitrogen, NY) for 1 h. The cells were washed again with PBS and stained with DAPI. The location of Pc 4 (670 nm), EGF-Alexa 555 (594 nm), Tf-Alexa 488 (488 nm), or anti-LAMP2 (488 nm) was visualized using a Leica DM 4000B microscope at 40× magnification. The images were analyzed for intensities and Pearson correlation coefficients (PCC) using Leica application software (Leica Microsystems, IL) and ImageJ software (NIH, MA) for colocalization analysis.

PDT Assay

For dark and light assay, 30 000 U87 cells were plated in a 96-well plate. The cells were incubated for 4 h at 37 °C with increasing concentrations of (EGF_{pep}+Tf_{pep})-AuNPs (1–1000 nM) and compared to free Pc 4 at the same concentrations (in phenol red-free medium). After incubation, the cells were washed with fresh media. The dark assay was kept in the incubator for another 24 h without exposure to the PDT 670 nm laser. The light assay was irradiated with a 670 nm laser (500 J cm^{-2}) for 10 min at a fluence rate of 0.83. The cells were incubated for an additional 24 h. Phase contrast images of the dark and light assay were taken using a Leica DMIL LED microscope (Leica Microsystems, IL). Cell viability studies were carried out using Guava Easycyte 8HT (EMD Millipore, MA). The cells were trypsinized and stained with Guava Viacount Reagent for 15 min prior to the analysis. The viability assay collected 1000 cellular events per well at a steady flow rate of 0.59 uL s^{-1}.

Tumor Implantation

Female athymic mice were obtained from the NIH NCI. Human glioma (U87) cancer cell lines overexpressing both EGFR and TfR were implanted into the brain cortex of athymic mice (3×10^5 cells per implant). Tumors developed for 9 days prior to systemic injection with AuNPs-Pc 4 conjugates. Animals were fed exclusively on a special rodent diet (Tekland 2018S; Harlan Laboratories, Inc., IN) to reduce autofluorescence. Animal experiments were performed according to Institutional Animal Care and Use Committee (IACUC) approved policies and guidelines at the Medical University of South Carolina (MUSC). The housing, feeding, and care of animals used for these experiments were directed by veterinarians on staff at MUSC, trained and experienced in the proper care, handling, and use of the mice. Research was conducted in compliance with the Animal Welfare Act and other federal statutes and regulations pertaining to animals and experiments

involving animals, and adheres to principles stated in the Guide for the Care and Use of Laboratory Animals, NRC publication, 2011 edition.

In Vivo Fluorescence Imaging

Mice bearing orthotopic tumors derived from U87-MG cells were injected with the compounds mixed in saline (N = 3 per each AuNPs group) at 1 mg kg^{-1} Pc 4 via tail vein injection. Before injection, mice were anesthetized with isoflurane and subjected to spectral fluorescence imaging. Animals were reimaged after 1 h over a 24 h period. Fluorescent multispectral images were obtained using the Maestro *in vivo* Imaging System (PerkinElmer, MA). The orange filter set appropriate for Pc 4 was used for emission and excitation light. The tunable filter was automatically stepped in 10 nm increments, whereas the camera captured images at a constant exposure of 1000 ms. Fluorescence images were acquired before treatment, immediately after, and 6 h after treatment. Spectral libraries were generated by assigning spectral peaks to background and fluorescence probe on tissue. The spectral libraries were manually computed using the Maestro software, with each tissue used as its own background control. To compare signal intensities, ROIs were selected over the tumor or nontumor areas, and the change in fluorescence signal over baseline was determined. The spectral fluorescent images consisting of autofluorescence spectra and imaging probe were captured and unmixed on the basis of their spectral patterns. The total signal in the ROI (defined as photons per second) was divided by the area.

RESULTS

To produce hydrophobic AuNPs (Figure 1a), we used a modified Brust–Schiffrin synthesis scheme, and the size of the AuNPs was characterized by TEM.[24,32,33] Figure 1, panels b and c show a representative TEM micrograph and size histogram of the hydrophobic AuNPs, respectively. The core diameter of the AuNPs was found to be 5.1 ± 0.6 nm. The TEM image exhibited a negligible contrast from the capped TOAB layer, and the particles were well-dispersed and not aggregated. Hydrophobic AuNPs, PEGylated AuNPs, EGF_{pep}-AuNPs, Tf_{pep}-AuNPs, AuNPs-Pc 4, and (EGF_{pep}+Tf_{pep})-AuNPs-Pc 4 were analyzed by DLS and were found to have average hydrodynamic diameters of 8.2 ± 1.2 nm, 10.1 ± 1.8 nm, 12.3 ± 2.1 nm, 12.5 ± 2.3 nm, 39 ± 3.5 nm, and 41 ± 6.2 nm, respectively, with a low PDI = 0.1 (Figure 1d, left graph).

To confirm loading of Pc 4 on the untargeted and targeted AuNPs, Pc 4 absorption was observed at 679 nm (Figure 1d, right graph). To calculate the number of Pc 4 molecules per AuNP, the absorption value of Pc 4 at 630 nm (ε = 2e5 M^{-1} cm^{-1}) and the absorption value of AuNPs at 520 nm (ε = 2.737e7 M^{-1} cm^{-1}) were measured. To calculate the concentration of Pc 4 per AuNP, Lamberts-beer law was utilized (A = εcl). The contribution of Au absorption at 630 nm was subtracted from the Pc 4 absorption (630 nm). The calculations based on the UV–vis spectra confirmed that approximately 20 Pc 4 molecules were adsorbed per AuNP.

To estimate the number of peptides on the AuNP, the surface area (SA) of a 5 nm AuNP (assumed to be a sphere) was calculated. This value was divided by 0.22 nm^2 (theoretical SA occupied by a single thiol ligand on the NP surface) to give the total number of possible

ligands per particle. On the basis of the stoichiometric molar ratio of (1:4) bifunctional to monofunctional PEGs, 20% of the total PEGs are bifunctional PEGs. Assuming peptide coupling was 100% efficient on the bifunctional PEGs, the final number of peptides is derived. We deduce that approximately 78 peptides were conjugated onto the surface of the AuNP. In the dual-targeted AuNPs, approximately 39 EGF_{pep} and 39 Tf_{pep} were conjugated to the surface to maintain a constant number of total peptides per AuNP.

Gel electrophoresis studies illustrated the surface charges of the various AuNPs and adsorption of the Pc 4 onto the AuNPs (Figure S1). The particles moved toward the positive electrode in an agarose gel electrophoresis experiment, indicating successful PEGylation and charge characteristics of the AuNPs (Figure S1, left panel). PEGylation transforms the hydrophobic AuNPs to negatively charged hydrophilic AuNPs. Pc 4 adsorption onto AuNPs is verified by the fluorescence in the agarose gel (Figure S1a). Measurement of zeta potential further confirms the negative charge of AuNPs observed during gel electrophoresis (Figure S1b). The Pc 4 remains in the wells, as observed by fluorescence, and is presumed to be due to the hydrophobic interactions of the drug with the hydrophobic polymerized agarose matrix[34] since the drug is not covalently bound to the AuNPs but instead adsorbed. Electric mobility shifts only the AuNPs toward the positive electrode, leaving the Pc 4 behind.

Drug-loaded AuNPs were evaluated for loading stability using UV–vis spectroscopy (Figure 1e). AuNPs-Pc 4 incubated in buffered solution over a 24 h period at room temperature (25 °C) lost on average one Pc 4 molecule per AuNP. In comparison, (EGF_{pep}+Tf_{pep})-AuNPs did not lose Pc 4 over the same time period. Under these buffered conditions, Pc 4 does not leach from the AuNPs.

We examined glioma cells for overexpression of multiple target receptors that would assist in improving specificity of the NPs. Glioma cells express EGFR and TfR at different levels. The U87 cell line expressed elevated levels of EGFR when compared to LN229 cells as shown by Western blot (Figure S2). Both cell lines expressed similar levels of TfR. Immunofluorescence confirms the overexpression of EGFR and TfR in U87 and LN229 cells (Figure S2).

The short-term kinetics of (EGF_{pep}+Tf_{pep})-AuNPs uptake in U87 (elevated EGFR and TfR) or LN229 (elevated TfR only) cells was studied using live cell microscopy. Images were taken every 15 min during a 1 h incubation period (Figure 2a). Pc 4 fluorescence was visible within the cells after 15 min of incubation. Pc 4 levels increased almost linearly with time in U87 cells incubated with (EGF_{pep}+Tf_{pep})-AuNPs (Figure 2b).

During a 24 h period, maximal (EGF_{pep}+Tf_{pep})-AuNPs-Pc 4 accumulation *in vitro* was observed within 1 h in the U87 cells, which is significantly faster (5–6-fold) than in cells treated with untargeted AuNPs (Figure 2c), while monotargeted AuNPs only exhibited a 2–3-fold increase over untargeted AuNPs (Figure 2d). Maximal levels of the monotargeted AuNPs (Tf_{pep}-AuNPs or EGF_{pep}-AuNPs) were seen between 4 and 8 h, respectively. In comparison, LN229 cells with fewer EGFR treated over a short period (1 h) with (EGF_{pep}+Tf_{pep})-AuNPs accumulated Pc 4 at a slower, less uniform rate (Figure 2b). After

45 min, (EGF_{pep}+Tf_{pep})-AuNPs were taken up in the LN229 cells but only two-fold more than untargeted AuNPs. In all cases, once maximal accumulation was reached, the amount of Pc 4 remained relatively constant.

To illustrate targeting specificity of the (EGF_{pep}+Tf_{pep})-AuNPs-Pc 4 for both cell surface receptors and demonstrate internalization, U87 cells with high endogenous levels of EGFR and TfR were incubated with (EGF_{pep}+Tf_{pep})-AuNPs-Pc 4 and a combination of the fluorescent conjugates of full length EGF protein (EGF-Alexa 555) and Tf protein (Tf-Alexa 488) (Figure 3a). The fluorescent conjugates of the full-length proteins minimally interfered with binding and internalization of the targeted AuNPs at time points less than 1 h.[35,36] Within 15 min, a subset of endosomes was identified as containing both EGF and Tf. These endosomes also contained Pc 4 as indicated by yellow in overlay images.

To quantify the colocalization between (EGF_{pep}+Tf_{pep})-AuNPs-Pc 4 and EGF containing vesicles or (EGF_{pep}+Tf_{pep})-AuNPs-Pc 4 and Tf containing vesicles, the number of colocalized fluorescence pixels using Pearson's correlation coefficient (PCC) was plotted over time (Figure 3b). Nonspecific colocalization was calculated based on the correlation of Pc 4 and the nuclear stain DAPI. No correlation was found between Pc 4 and the nucleus (PCC = −0.13 ± 0.106). As visualized, Pc 4 colocalized within vesicles containing either EGF or Tf as early as 5 min (PCC of 0.78 and 0.58, respectively) and reached maximal levels within 15 min (PCC 0.83 and 0.72, respectively) (Figure 3b, black arrows). The percent of Pc 4 colocalized with EGF pixels was slightly higher (80%) than that of Pc 4 colocalized with Tf pixels (57–72%). The number of colocalized Pc 4 and EGF pixels remained fairly constant, whereas the number of colocalized Pc 4 and Tf pixels decreased, likely due to the trafficking of Tf to a different postendocytotic degradation pathway.

However, we surmised that (EGF_{pep}+Tf_{pep})-AuNPs-Pc 4 would be internalized into enriched-vesicles containing both EGF and Tf as a smaller subset of the individual vesicles (Figure 3c). We measured the colocalization of Pc 4 with EGF and Tf vesicles over time and then calculated the correlation of signal overlap based on the number of EGF and Tf containing endosomes. Pc 4 appeared to correlate simultaneously with EGF and Tf-enriched endosomes in approximately 34% of the vesicles at the earliest time point (5 min). At 15 min, approximately 58% of the combined vesicles also contained Pc 4. The correlation decreased after 30 min in a pattern similar to that of Pc 4 in Tf-enriched vesicles.

Glioma cells were incubated with (EGF_{pep}+Tf_{pep})-AuNPs-Pc 4 over increasing time, fixed, and immunostained for lysosomes. Fluorescence images showed that (EGF_{pep}+Tf_{pep})-AuNPs-Pc 4 colocalization within the lysosomes after 1 h was negligible (Figure 3d). The degree of colocalization was measured as less than 20%.

To further demonstrate specificity of the two targeting moieties conjugated to the AuNPs, we conducted a competition experiment of (EGF_{pep}+Tf_{pep})-AuNPs-Pc 4 against the targeting full-length growth factors, either individually or in concert (Figure 4). U87 cells were treated with dual-targeted AuNPs in the absence (media) or presence of full-length EGF, Tf, or a combination of both EGF and Tf. After 1 h of incubation, the accumulation of Pc 4 is inhibited by 15% when U87 cells are treated with EGF alone, by 26% when treated

with Tf alone, and by 46% when treated with EGF and Tf together. The inhibition significantly increases to 82% when the incubation time is increased to 4 h in the presence of both EGF and Tf (red bar). This confirms the selective and specific nature of (EGF_{pep}+Tf_{pep})-AuNPs-Pc 4 for targeting tumor cells with overexpressed receptors.

Activation of the photosensitizer delivered intracellularly by the AuNPs takes place by laser excitation of Pc 4 at 670 nm; subsequent cell death can be measured by cell viability assays. To evaluate efficacy of AuNPs-delivered Pc 4, PDT experiments were conducted after a 4 h treatment with increasing concentrations (0–1000 nM) of (EGF_{pep}+Tf_{pep})-AuNPs-Pc 4 and compared to those of free Pc 4. Regardless of whether the cells were treated with free Pc 4 or (EGF_{pep}+Tf_{pep})-AuNPs-Pc 4, the U87 cells remained healthy without light activation of the Pc 4 (dark assay) as visualized by phase contrast microscopy of the cellular morphology (Figure 5a). Upon light activation (670 nm, light assay), the cells treated with 100 nM of (EGF_{pep}+Tf_{pep})-AuNPs-Pc 4 showed significant cell death (40% reduction) when compared to the same concentration of free Pc 4 (Figure 5b). In contrast, free Pc 4 does not show significant cell cytotoxicity until treated with 1000 nM (60% reduction), at which point the toxicity is similar to that of cells treated with (EGF_{pep}+Tf_{pep})-AuNPs-Pc 4 (81% reduction). (EGF_{pep}+Tf_{pep})-AuNPs-Pc 4 is more efficient than free Pc 4 at lower concentrations, illustrating the competence of these AuNPs to induce cell death after drug delivery.

In addition, a comparison study of cellular cytotoxicity after treatment of glioma cells with either single- or dual-targeted AuNPs was conducted (Figure S3). As shown, once the targeted AuNPs (whether single or dual targeted) delivered Pc 4 to the cells and the drug was internalized, activation with light of the Pc 4 efficiently kills the cells at comparable levels at 100 nM, with dual targeting slightly better at higher (1000 nM) concentrations. These data suggest that targeting of the AuNPs is decoupled from the killing efficacy and merely improves cell specificity.

Finally, to test whether or not the (EGF_{pep}+Tf_{pep})-AuNPs-Pc 4 were able to cross the BBB, mice were orthotopically implanted with U87 cells and intravenously injected with either Au-NPs-Pc 4 or (EGF_{pep}+Tf_{pep})-AuNPs-Pc 4 [1 mg kg^{-1} Pc 4]. The cranium was imaged from 1 to 24 h after intravenous injection with targeted or untargeted AuNPs-Pc 4 (Figure 6a). Spectral analysis revealed Pc 4 delivered by (EGF_{pep}+Tf_{pep})-AuNPs-Pc 4 reached maximal accumulation by 4 h. The overlap in delivery and release dynamics *in vivo* supports the contention that the most suitable time for accumulation is within 4 h. Spectrally separated Pc 4 images of the dorsal cranium of mice implanted with an orthotopic brain tumor injected with either (EGF_{pep}+Tf_{pep})-AuNPs-Pc 4 or AuNPs-Pc 4 were quantified using Maestro imaging software (Figure 6b). (EGF_{pep}+Tf_{pep})-AuNPs-Pc 4 injected mice accumulated significant amounts of Pc 4 rapidly, while AuNPs-Pc 4 injected mice took up less drug over the same period. As reported in previous studies, by 24 h, the AuNPs were excreted from the kidney with some accumulation remaining in the liver (Figure S4).[24,37] In the organs of mice injected with untargeted AuNPs and allowed to circulate over 24 h, the Pc 4 accumulated within the liver, kidney, and spleen at very low levels. When compared to dual-targeted AuNPs, almost no Pc 4 remained with minimal Pc 4 observed in the liver.

DISCUSSION

The purpose of this study was to develop a multitargeted NP to help identify brain tumors and deliver drug more specifically. We synthesized hydrophobic AuNPs to enable the loading of hydrophobic Pc 4 drug in the final step. Solubility in aqueous solution was achieved via PEGylation followed by attachment of EGF_{pep} and Tf_{pep} and finally loading of Pc 4 in organic solvent (Figure 1a). Loading of Pc 4 on the targeted AuNPs increased the size of the AuNPs to 41 ± 6.2 nm due to the insertion of the drug inside the PEG corona, increasing steric hindrance and pulling the PEG apart. To further explain the size difference of ~30 nm, when Pc 4 was adsorbed, theoretical calculations were carried out. Differences between the SA of PEGylated and Pc 4-loaded AuNPs were calculated and compared with the SA of 20 Pc 4 molecules. Twenty Pc 4 molecules displace a SA on the PEG corresponding to a sphere of around 32 nm in diameter. DLS size distribution is identical to the instrumental response function corresponding to a monodispersed sample, indicating that aggregation is negligible. It is noteworthy that the calculated hydrodynamic diameter is slightly larger than the actual diameter because of the counterion cloud contributions to particle mobility.[38]

Similar to our findings, reduced thioctic acid–lisinopril AuNPs in PBS showed stability up to 7 days as observed by UV–vis spectroscopy.[39] In another study, doxorubicin (DOX)-PEGylated thiol-coated AuNPs demonstrated negligible drug release at pH 7, thereby indicating the robust nature of thiol–Au bond.[40] DOX-conjugated AuNPs were stable during circulation and released in the tumor proximity due to lowered pH environment. Another study entails good stability of curcumin-coated AuNPs at physiological pH.[41] Curcumin release was also observed in an acidic environment of glioma cells. This validates the stability of the thiol bond (S–Au) in AuNP conjugates as utilized in (EGF_{pep}+Tf_{pep})-AuNPs loaded with Pc 4.

To achieve efficient and specific drug delivery into cells, the most promising strategies involve utilizing various targeting moieties or ligands that bind specifically to a cell's surface. The vast majority of targeting is achieved by monotarget functionalization of the NPs.[24,29,37] Recently, we and others have begun to functionalize the NPs with more than one target. Several targeting moiety combinations have been utilized including ligands, extracellular proteins, aptamers,[42] peptides,[43,44] and antibodies. To date, these multitargeted NPs have concentrated on targeting two different cell types within the same local region. However, targeting to improve specificity within a single cancer cell type that is prone to extreme heterogeneity of overexpressed cell surface receptors within a tumor has not been well addressed until now.

Gel electrophoresis studies and measurements of zeta potential demonstrated that (EGF_{pep}+Tf_{pep})-AuNPs were negatively charged, indicating that uptake of the AuNPs was orchestrated by internalization of the targeting peptides. This is in contrast to positively charged particles, which are more successfully and nonspecifically phagocytosed by cells.[45] Pc 4 also leached from the particle during electrophoresis, supporting the hydrophobic interaction of the drug with the PEGylated AuNP.

The EGF_{pep} (YHWYGYTPQNVI) is a peptide screened from a phage display peptide library.[46] This peptide attaches specifically and efficiently to EGFR ($K_d \approx 22$ nM) with lower mitogenic activity compared to EGF alone. In another phage display system, Engler et al. identified Tf_{pep} (HAIYPRH), which binds through a cavity on the surface of receptor not within the active site, and it is internalized via endocytosis.[47] The peptide binds to the TfR in a dose-dependent manner with a K_d of ~10 nM, similar to that of holo-transferrin.

Both EGF_{pep} and Tf_{pep} bind to their respective receptors and are internalized.[46,48,49] Because of the varied cell surface expression and internalization rates of each single receptor, it is difficult to investigate the synergistic impact of multiple targeting peptides. However, it is anticipated that (EGF_{pep}+Tf_{pep})-AuNPs loaded with Pc 4 would follow a similar receptor-mediated endocytosis with receptor sorting occurring after internalization. Our data showed that the (EGF_{pep}+Tf_{pep})-AuNPs-Pc 4 were taken up via receptor-mediated endocytosis better than single-targeted AuNPs. Micrographs also revealed that the Pc 4 quickly unloaded from the internalized AuNPs and is found throughout the cytoplasm after 1 h. By examining the targeted AuNPs after internalization, there appeared to be a decrease in correlation that is probably due to further sorting of the two individual vesicles. This is expected based on numerous studies that concluded that EGF and Tf are internalized into similar endocytotic vesicles, which fuse with a sorting endosome and from which Tf complexes are later removed for recycling.[50,51] In comparison, EGF undergoes a more complex vesiculation pathway.[52]

AuNPs coated with PEG could affect multivalency and avidity of the targeting. In principle, each targeting moiety is readily tunable and replaceable. The presence of the PEG layer on the AuNPs does not affect binding affinity and specificity of the dual-targeted AuNPs. In *in vivo* experiments, targeting both EGFR and TfR on the same NP showed excellent selectivity to brain tumors that overexpressed both receptors as compared to AuNPs that are targeted using single targeting moieties.[24,29] The amount of (EGF_{pep}+Tf_{pep})-AuNPs-Pc 4 reached its highest levels at 4 h post injection, whereas untargeted AuNPs washed out rapidly, clearing the tumor within 24 h.

CONCLUSIONS

In summary, this work illustrates a development of dual-targeted AuNPs designed to deliver hydrophobic drugs like photosensitizers to brain tumors. These dual-targeted NPs were 5–6-fold more effective at delivering Pc 4 inside cells as compared to untargeted and were a significant improvement over single-targeted AuNPs. Receptor-mediated endocytosis of these AuNPs in EGF and Tf containing endosomes was confirmed by colocalization studies, which suggest an active, selective accumulation and sorting within the cell. Upon activation of Pc 4 in PDT cytotoxicity experiments, dual-targeted AuNPs were more effective than free Pc 4 at lower than standard of care concentrations. Furthermore, these targeted NPs were able to traverse the BBB more efficiently as compared to untargeted AuNPs, leading to higher accumulation levels at a faster rate. All these findings point to the potential of a multifunctional drug delivery system, which can easily cross the BBB, selectively target the malignant tumor cells, and reduce untoward photosensitizer cytotoxicity within the surrounding milieu.

Supplementary Material

Refer to Web version on PubMed Central for supplementary material.

ACKNOWLEDGMENTS

This work was supported by Grant No. R01EB012099 from the National Institute of Biomedical Imaging and Bioengineering (NIBIB). The content and views are solely the responsibility of the authors and do not necessarily represent the official views of the NIBIB or the National Institutes of Health.

ABBREVIATIONS

AuNPs	gold nanoparticles
BBB	blood brain barrier
DLS	dynamic light scattering
EGF	epidermal growth factor
EGFR	epidermal growth factor receptor
GBM	glioblastoma multiform
NP	nanoparticle
Pc 4	phthalocyanine 4
PCC	Pearson’s correlation coefficient
PDT	photodynamic therapy
PEG	polyethylene glycol
QD	quantum dot
SA	surface area
Tf	transferrin
TfR	transferrin receptor
UV–vis	ultraviolet–visible spectroscopy

REFERENCES

(1). Huse JT, Holland EC. Targeting brain cancer: advances in the molecular pathology of malignant glioma and medulloblastoma. Nat. Rev. Cancer. 2010; 10(5):319–31. [PubMed: 20414201]

(2). Jansen M, de Witt Hamer PC, Witmer AN, Troost D, van Noorden CJ. Current perspectives on antiangiogenesis strategies in the treatment of malignant gliomas. Brain Res. Rev. 2004; 45(3): 143–63. [PubMed: 15210301]

(3). Pardridge WM. Drug and gene targeting to the brain with molecular Trojan horses. Nat. Rev. Drug Discov. 2002; 1(2):131–9. [PubMed: 12120094]

(4). Huynh GH, Deen DF, Szoka FC Jr. Barriers to carrier mediated drug and gene delivery to brain tumors. J. Controlled Release. 2006; 110(2):236–59.

(5). Zhang L, Gu FX, Chan JM, Wang AZ, Langer RS, Farokhzad OC. Nanoparticles in medicine: therapeutic applications and developments. Clin. Pharmacol. Ther. 2008; 83(5):761–9. [PubMed: 17957183]

(6). Whitesides GM. The 'right' size in nanobiotechnology. Nat. Biotechnol. 2003; 21(10):1161–5. [PubMed: 14520400]

(7). Youns M, Hoheisel JD, Efferth T. Therapeutic and diagnostic applications of nanoparticles. Curr. Drug Targets. 2011; 12(3):357–65. [PubMed: 20955146]

(8). Nune SK, Gunda P, Thallapally PK, Lin YY, Forrest ML, Berkland CJ. Nanoparticles for biomedical imaging. Expert Opin. Drug Delivery. 2009; 6(11):1175–94.

(9). Jain KK. Use of nanoparticles for drug delivery in glioblastoma multiforme. Expert Rev. Neurother. 2007; 7(4):363–72. [PubMed: 17425491]

(10). Hadjipanayis CG, Machaidze R, Kaluzova M, Wang L, Schuette AJ, Chen H, Wu X, Mao H. EGFRvIII antibody-conjugated iron oxide nanoparticles for magnetic resonance imaging-guided convection-enhanced delivery and targeted therapy of glioblastoma. Cancer Res. 2010; 70(15): 6303–12. [PubMed: 20647323]

(11). Dilnawaz F, Singh A, Mewar S, Sharma U, Jagannathan NR, Sahoo SK. The transport of non-surfactant based paclitaxel loaded magnetic nanoparticles across the blood brain barrier in a rat model. Biomaterials. 2012; 33(10):2936–51. [PubMed: 22264522]

(12). Faucher L, Guay-Begin AA, Lagueux J, Cote MF, Petitclerc E, Fortin MA. Ultra-small gadolinium oxide nanoparticles to image brain cancer cells in vivo with MRI. Contrast Media Mol. Imaging. 2010; 6(4):209–18. [PubMed: 21861281]

(13). Park JY, Baek MJ, Choi ES, Woo S, Kim JH, Kim TJ, Jung JC, Chae KS, Chang Y, Lee GH. Paramagnetic ultrasmall gadolinium oxide nanoparticles as advanced T1MRI contrast agent: account for large longitudinal relaxivity, optimal particle diameter, and in vivo T1MR images. ACS Nano. 2009; 3(11):3663–9. [PubMed: 19835389]

(14). Huang J, Xie J, Chen K, Bu L, Lee S, Cheng Z, Li X, Chen X. HSA coated MnO nanoparticles with prominent MRI contrast for tumor imaging. Chem. Commun. (Cambridge, U. K.). 2010; 46(36):6684–6.

(15). Bennewitz MF, Lobo TL, Nkansah MK, Ulas G, Brudvig GW, Shapiro EM. Biocompatible and pH-sensitive PLGA encapsulated MnO nanocrystals for molecular and cellular MRI. ACS Nano. 2011; 5(5):3438–46. [PubMed: 21495676]

(16). Shubayev VI, Pisanic TR 2nd, Jin S. Magnetic nanoparticles for theragnostics. Adv. Drug Delivery Rev. 2009; 61(6):467–77.

(17). Popescu MA, Toms SA. In vivo optical imaging using quantum dots for the management of brain tumors. Expert Rev. Mol. Diagn. 2006; 6(6):879–90. [PubMed: 17140375]

(18). Jackson H, Muhammad O, Daneshvar H, Nelms J, Popescu A, Vogelbaum MA, Bruchez M, Toms SA. Quantum dots are phagocytized by macrophages and colocalize with experimental gliomas. Neurosurgery. 2007; 60(3):524–9. discussion 529–30. [PubMed: 17327798]

(19). Cheng Y, Samia AC, Meyers JD, Panagopoulos I, Fei B, Burda C. Highly efficient drug delivery with gold nanoparticle vectors for in vivo photodynamic therapy of cancer. J. Am. Chem. Soc. 2008; 130(32):10643–7. [PubMed: 18642918]

(20). Ghosh P, Han G, De M, Kim CK, Rotello VM. Gold nanoparticles in delivery applications. Adv. Drug Delivery Rev. 2008; 60(11):1307–15.

(21). Paciotti GF, Myer L, Weinreich D, Goia D, Pavel N, McLaughlin RE, Tamarkin L. Colloidal gold: a novel nanoparticle vector for tumor directed drug delivery. Drug Delivery. 2004; 11(3): 169–83. [PubMed: 15204636]

(22). Kim CK, Ghosh P, Pagliuca C, Zhu ZJ, Menichetti S, Rotello VM. Entrapment of hydrophobic drugs in nanoparticle monolayers with efficient release into cancer cells. J. Am. Chem. Soc. 2009; 131(4):1360–1. [PubMed: 19133720]

(23). Choi CH, Alabi CA, Webster P, Davis ME. Mechanism of active targeting in solid tumors with transferrin-containing gold nanoparticles. Proc. Natl. Acad. Sci. U. S. A. 2010; 107(3):1235–40. [PubMed: 20080552]

(24). Cheng Y, Meyers JD, Agnes RS, Doane TL, Kenney ME, Broome AM, Burda C, Basilion JP. Addressing brain tumors with targeted gold nanoparticles: a new gold standard for hydrophobic drug delivery? Small. 2011; 7(16):2301–6. [PubMed: 21630446]

(25). Muragaki Y, Akimoto J, Maruyama T, Iseki H, Ikuta S, Nitta M, Maebayashi K, Saito T, Okada Y, Kaneko S, Matsumura A, Kuroiwa T, Karasawa K, Nakazato Y, Kayama T. Phase II clinical

study on intraoperative photodynamic therapy with talaporfin sodium and semiconductor laser in patients with malignant brain tumors. J. Neurosurg. 2013; 119(4):845–52. [PubMed: 23952800]

(26). Eljamel MS, Goodman C, Moseley H. ALA and Photofrin fluorescence-guided resection and repetitive PDT in glioblastoma multiforme: a single centre Phase III randomised controlled trial. Lasers Med. Sci. 2008; 23(4):361–7. [PubMed: 17926079]

(27). Dougherty TJ. An update on photodynamic therapy applications. J. Hematother. 2002; 20(1):3–7.

(28). Popovic EA, Kaye AH, Hill JS. Photodynamic therapy of brain tumors. J. Clin. Laser Med. Surg. 1996; 14(5):251–61. [PubMed: 9612191]

(29). Dixit S, Novak T, Miller K, Zhu Y, Kenney ME, Broome A-M. Transferrin receptor-targeted theranostic gold nanoparticles for photosensitizer delivery in brain tumors. Nanoscale. 2015; 7:1782–90. [PubMed: 25519743]

(30). Broome A-M, Bhavsar N, Ramamurthy G, Newton G, Basilion JP. Expanding the Utility of β-Galactosidase Complementation: Piece by Piece. Mol. Pharmaceutics. 2010; 7(1):60–74.

(31). Inda MM, Bonavia R, Mukasa A, Narita Y, Sah DW, Vandenberg S, Brennan C, Johns TG, Bachoo R, Hadwiger P, Tan P, Depinho RA, Cavenee W, Furnari F. Tumor heterogeneity is an active process maintained by a mutant EGFR-induced cytokine circuit in glioblastoma. Genes Dev. 2010; 24(16):1731–45. [PubMed: 20713517]

(32). Brust M, Walker M, Bethell D, Schiffrin DJ, Whyman R. Synthesis of thiol-derivatised gold nanoparticles in a two-phase Liquid-Liquid system. J. Chem. Soc., Chem. Commun. 1994; 7:801–802.

(33). Duan H, Nie S. Etching colloidal gold nanocrystals with hyperbranched and multivalent polymers: a new route to fluorescent and water-soluble atomic clusters. J. Am. Chem. Soc. 2007; 129(9):2412–3. [PubMed: 17295485]

(34). Fatin-Rouge N, Starchev K, Buffle J. Size Effects on Diffusion Processes within Agarose Gels. Biophys. J. 2004; 86(5):2710–2719. [PubMed: 15111390]

(35). Wang J, Xie X. Development of a quantitative, cell-based, high-content screening assay for epidermal growth factor receptor modulators. Acta Pharmacol. Sin. 2007; 28(10):1698–704. [PubMed: 17883960]

(36). Biswas S, Dodwadkar NS, Deshpande PP, Parab S, Torchilin VP. Surface functionalization of doxorubicin-loaded liposomes with octa-arginine for enhanced anticancer activity. Eur. J. Pharm. Biopharm. 2013; 84(3):517–25. [PubMed: 23333899]

(37). Cheng Y, Meyers JD, Broome AM, Kenney ME, Basilion JP, Burda C. Deep penetration of a PDT drug into tumors by noncovalent drug-gold nanoparticle conjugates. J. Am. Chem. Soc. 2011; 133(8):2583–91. [PubMed: 21294543]

(38). Fernandez-Nieves A, Fernandez-Barbero A, de las Nieves FJ. Particle-counterion clustering in highly charge-asymmetric complex fluids. Phys. Rev. E: Stat. Phys., Plasmas, Fluids, Relat. Interdiscip. Top. 2001; 63(4):041404.

(39). Ghann WE, Aras O, Fleiter T, Daniel M-C. Syntheses and Characterization of Lisinopril-Coated Gold Nanoparticles as Highly Stable Targeted CT Contrast Agents in Cardiovascular Diseases. Langmuir. 2012; 28(28):10398–10408. [PubMed: 22702239]

(40). Ruan S, Yuan M, Zhang L, Hu G, Chen J, Cun X, Zhang Q, Yang Y, He Q, Gao H. Tumor microenvironment sensitive doxorubicin delivery and release to glioma using angiopep-2 decorated gold nanoparticles. Biomaterials. 2015; 37(0):425–435. [PubMed: 25453970]

(41). Dey S, Sreenivasan K. Conjugating curcumin to water soluble polymer stabilized gold nanoparticles via pH responsive succinate linker. J. Mater. Chem. B. 2015; 3:824.

(42). Liu GX, Fang GQ, Xu W. Dual targeting biomimetic liposomes for paclitaxel/DNA combination cancer treatment. Int. J. Mol. Sci. 2014; 15(9):15287–303. [PubMed: 25177862]

(43). Gao H, Hu Y, Xiong Y, Zhang S, Yang J, Yu L, Jiang X. Glioma targeting and anti-glioma effect of interleukin 13 peptide and RGD peptide dual functionalized nanoparticles. Curr. Pharm. Biotechnol. 2014; 14(13):1118–26. [PubMed: 24016266]

(44). Rangger C, Helbok A, Sosabowski J, Kremser C, Koehler G, Prassl R, Andreae F, Virgolini IJ, von Guggenberg E. Decristoforo, C. Tumor targeting and imaging with dual-peptide conjugated multifunctional liposomal nanoparticles. Int. J. Nanomed. 2013; 8:4659–71.

(45). Yu SS, Lau CM, Thomas SN, Jerome WG, Maron DJ, Dickerson JH, Hubbell JA, Giorgio TD. Size- and charge-dependent non-specific uptake of PEGylated nanoparticles by macrophages. Int. J. Nanomed. 2012; 7:799–813.

(46). Li Z, Zhao R, Wu X, Sun Y, Yao M, Li J, Xu Y, Gu J. Identification and characterization of a novel peptide ligand of epidermal growth factor receptor for targeted delivery of therapeutics. FASEB J. 2005; 19(14):1978–85. [PubMed: 16319141]

(47). Oh S, Kim BJ, Singh NP, Lai H, Sasaki T. Synthesis and anti-cancer activity of covalent conjugates of artemisinin and a transferrin-receptor targeting peptide. Cancer Lett. 2009; 274(1): 33–9. [PubMed: 18838215]

(48). Agnes RS, Broome AM, Wang J, Verma A, Lavik K, Basilion JP. An optical probe for noninvasive molecular imaging of orthotopic brain tumors overexpressing epidermal growth factor receptor. Mol. Cancer Ther. 2012; 11(10):2202–11. [PubMed: 22807580]

(49). Lee JH, Engler JA, Collawn JF, Moore BA. Receptor mediated uptake of peptides that bind the human transferrin receptor. Eur. J. Biochem. 2001; 268(7):2004–12. [PubMed: 11277922]

(50). Dickson RB, Hanover JA, Willingham MC, Pastan I. Prelysosomal divergence of transferrin and epidermal growth factor during receptor-mediated endocytosis. Biochemistry. 1983; 22(24): 5667–74. [PubMed: 6317024]

(51). Hanover JA, Willingham MC, Pastan I. Kinetics of transit of transferrin and epidermal growth factor through clathrin-coated membranes. Cell. 1984; 39(2):283–93. [PubMed: 6149810]

(52). Hopkins CR, Gibson A, Shipman M, Miller K. Movement of internalized ligand-receptor complexes along a continuous endosomal reticulum. Nature. 1990; 346(6282):335–9. [PubMed: 2374607]

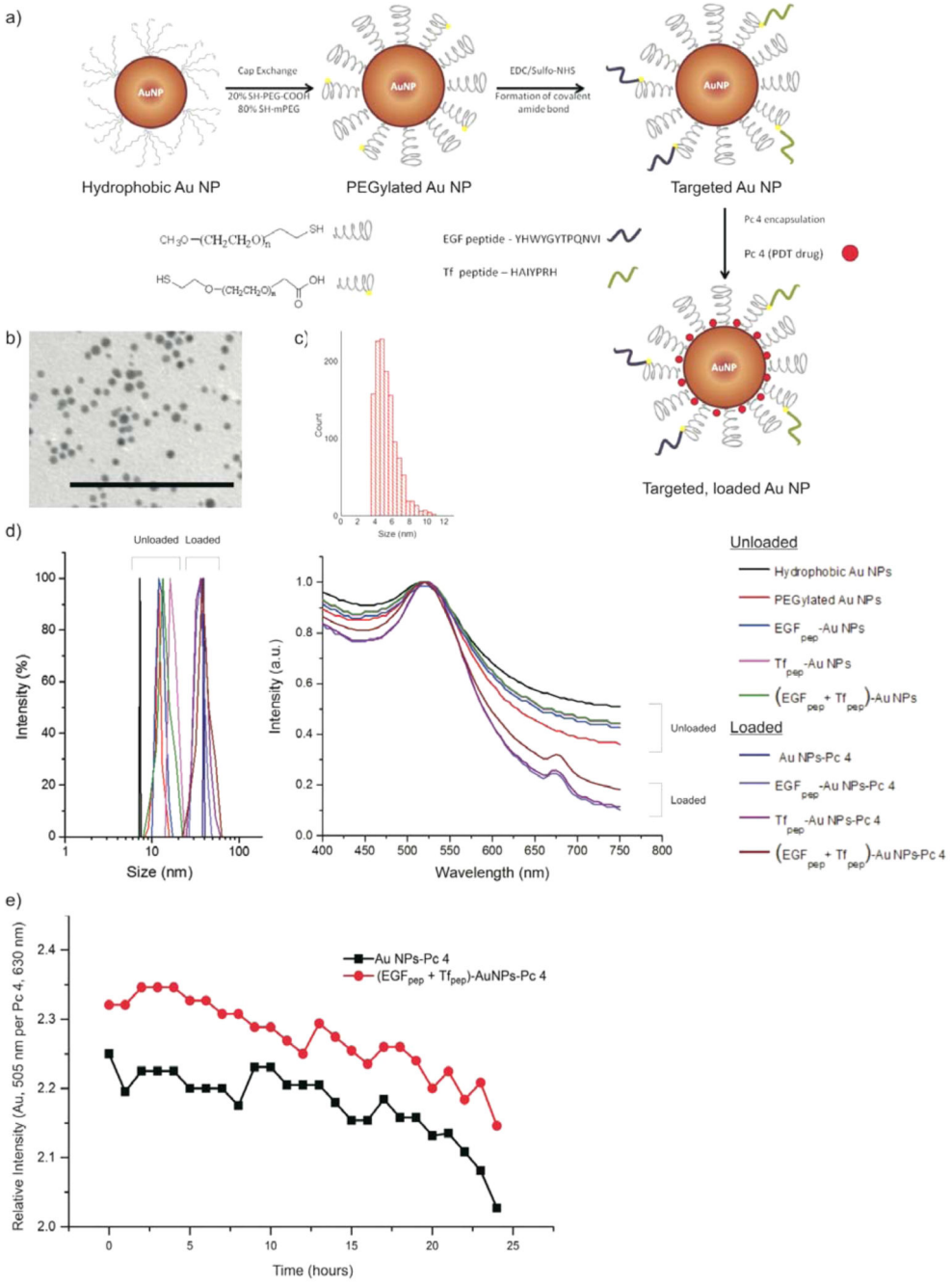

Figure 1.

Characterization of synthesized AuNPs. (a) Design of a dual-targeted AuNP loaded with Pc 4. (b) TEM of hydrophobic AuNPs. Scale bar = 100 nm. (c) Size histogram based on TEM micrographs. (d) DLS of AuNPs conjugates (left graph). UV–vis of AuNPs conjugates (right graph). (e) A 1% agarose gel at 120 V for 4 h in TAE (tris acetate EDTA) buffer. From left to right: (1) AuNPs-Pc 4, (2) EGF_{pep}-AuNPs-Pc 4, (3) Tf_{pep}-AuNPs-Pc 4, (4) (EGF_{pep}+Tf_{pep})-AuNPs-Pc 4. (f) Stability of targeted versus untargeted AuNPs in PBS over

time. Loss of Pc 4 per AuNP was measured as relative intensity of Pc 4 at 630 nm and compared to AuNP at 505 nm.

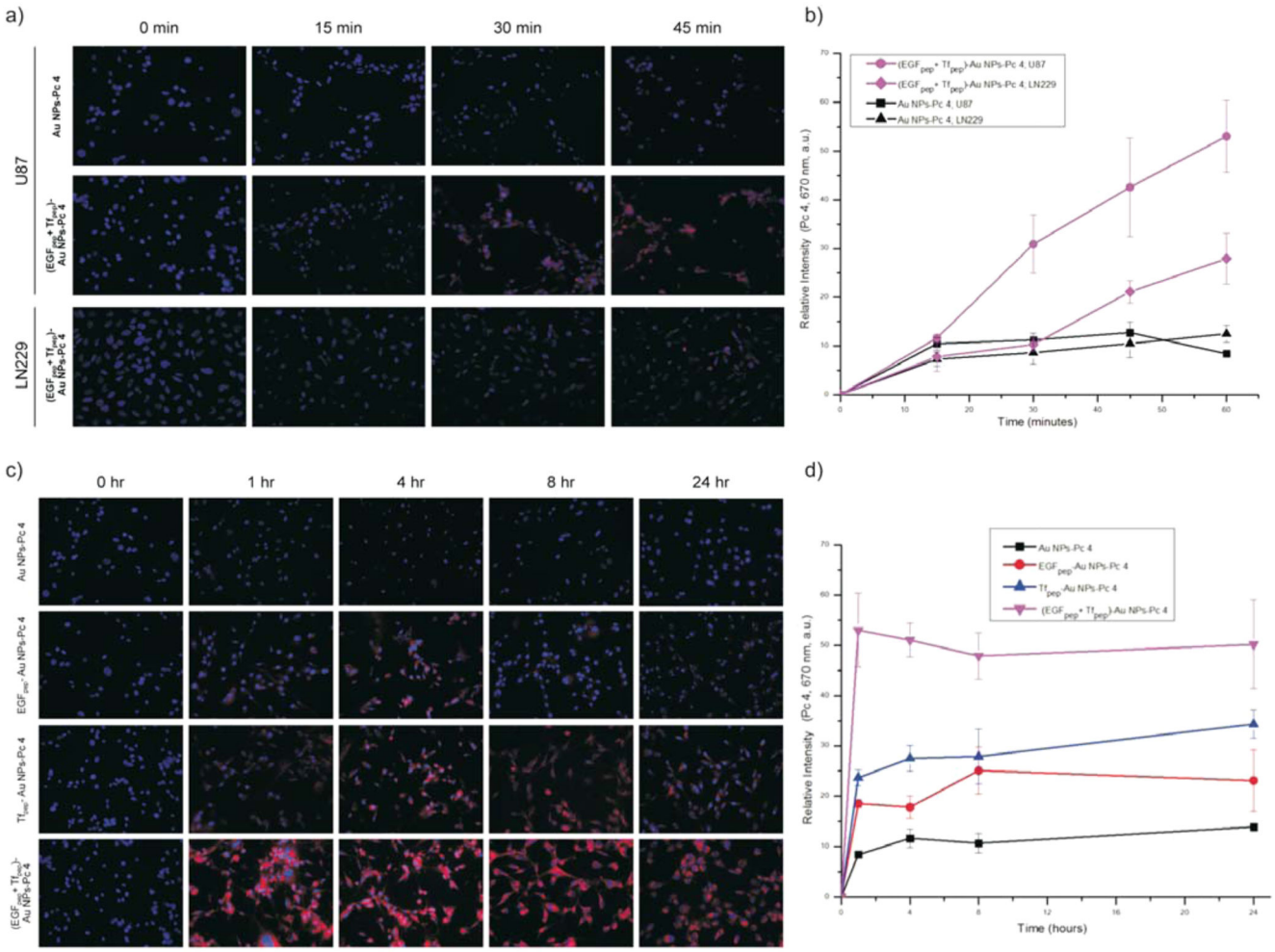

Figure 2.

Dual-targeted AuNPs-Pc 4 accumulate rapidly in glioma cell lines expressing both biomarkers. (a) Time course uptake of AuNPs conjugates (500 nM) in U87 and LN229 cell lines. Pc 4 fluorescence was acquired at 670 nm. (b) Relative intensities of Pc 4 versus time (0–60 min) for U87 and LN229 cells after treatment with either 500 nM of (EGF_{pep}+Tf_{pep})-AuNPs-Pc 4 or AuNPs-Pc 4. (c) Time course (0–24 h) uptake of single targeted AuNPs conjugates as compared to dual-targeted AuNPs in U87 cell line. (d) Quantification of Pc 4 accumulation over time measured as relative fluorescence.

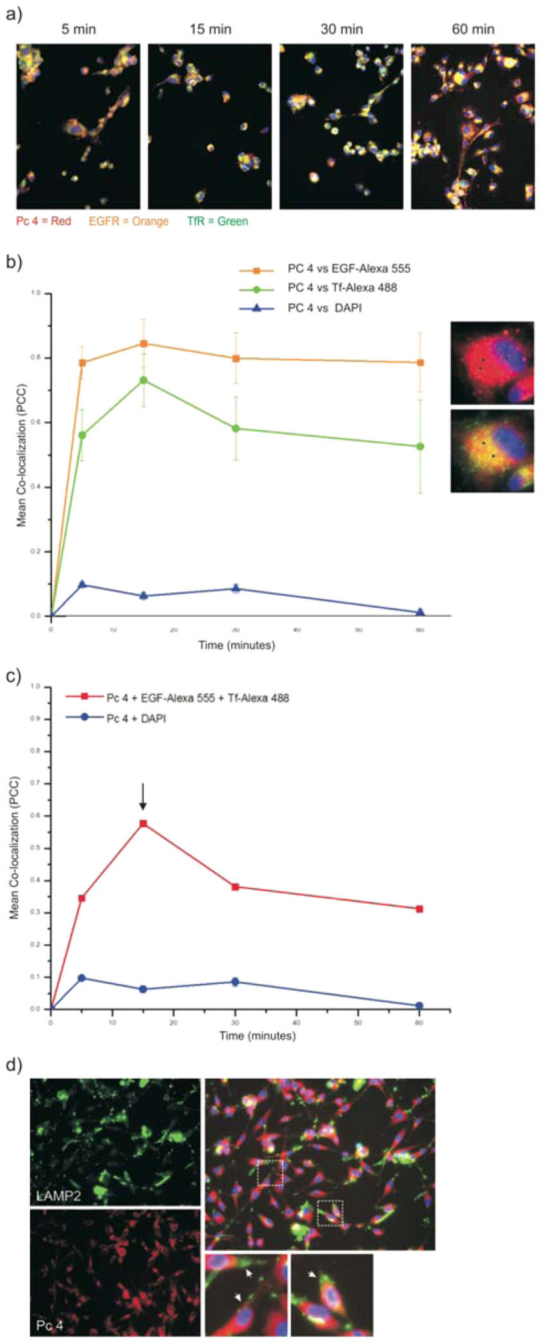

Figure 3.

Dynamics of (EGF_{pep}+Tf_{pep})-AuNPs-Pc 4 internalization and colocalization. (a) U87 cells were treated with (EGF_{pep}+Tf_{pep})-AuNPs-Pc 4 and EGF-Alexa 555 and Tf-Alexa 488 over increasing time. Individual channels were overlaid to identify colocalization of Pc 4-loaded AuNPs in EGFR and TfR containing vesicles (yellow). (b) Pc 4 sorted into vesicles containing EGF or Tf over time. Images are representative of 15 min. Black arrows = colocalization. (c) Signal overlap between both fluorophores and Pc 4 after increasing

incubation times. (d) (EGF_{pep}+Tf_{pep})-AuNPs-Pc 4-treated U87 cells were immunostained with anti-LAMP2 (green).

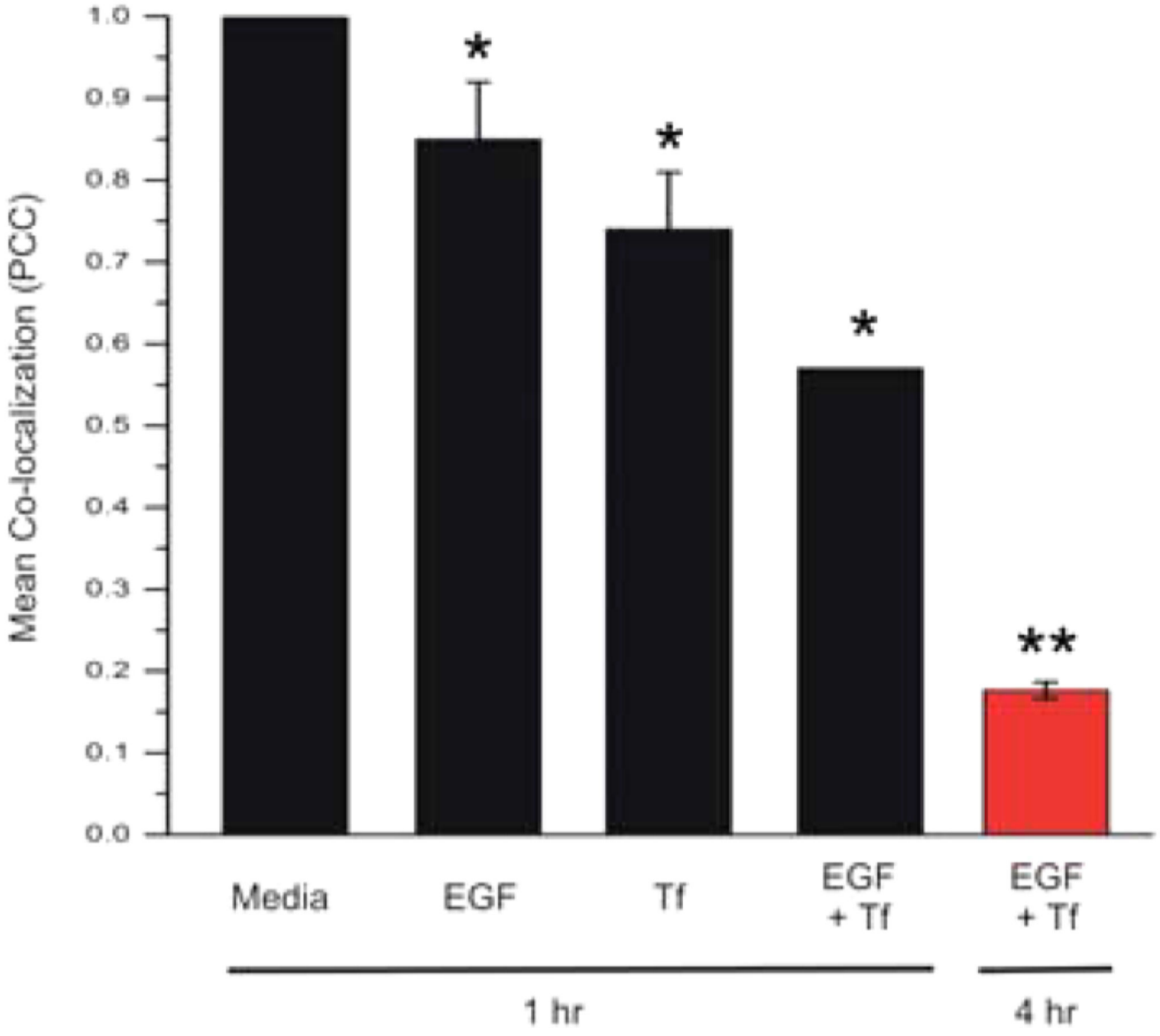

Figure 4.

Dual targeted AuNPs uptake is specific. U87 cells were incubated with targeted (EGF_{pep}+Tf_{pep})-AuNPs-Pc 4 (500 nM) and either fluorophore-conjugated full-length EGF (100 nM) or Tf (250 nM) or both EGF and Tf for 1 h (black bars) or 4 h (red bar). Pc 4 was measured by fluorescence (630 nm). (*, $p \leq 0.01$; **, $p \leq 0.001$).

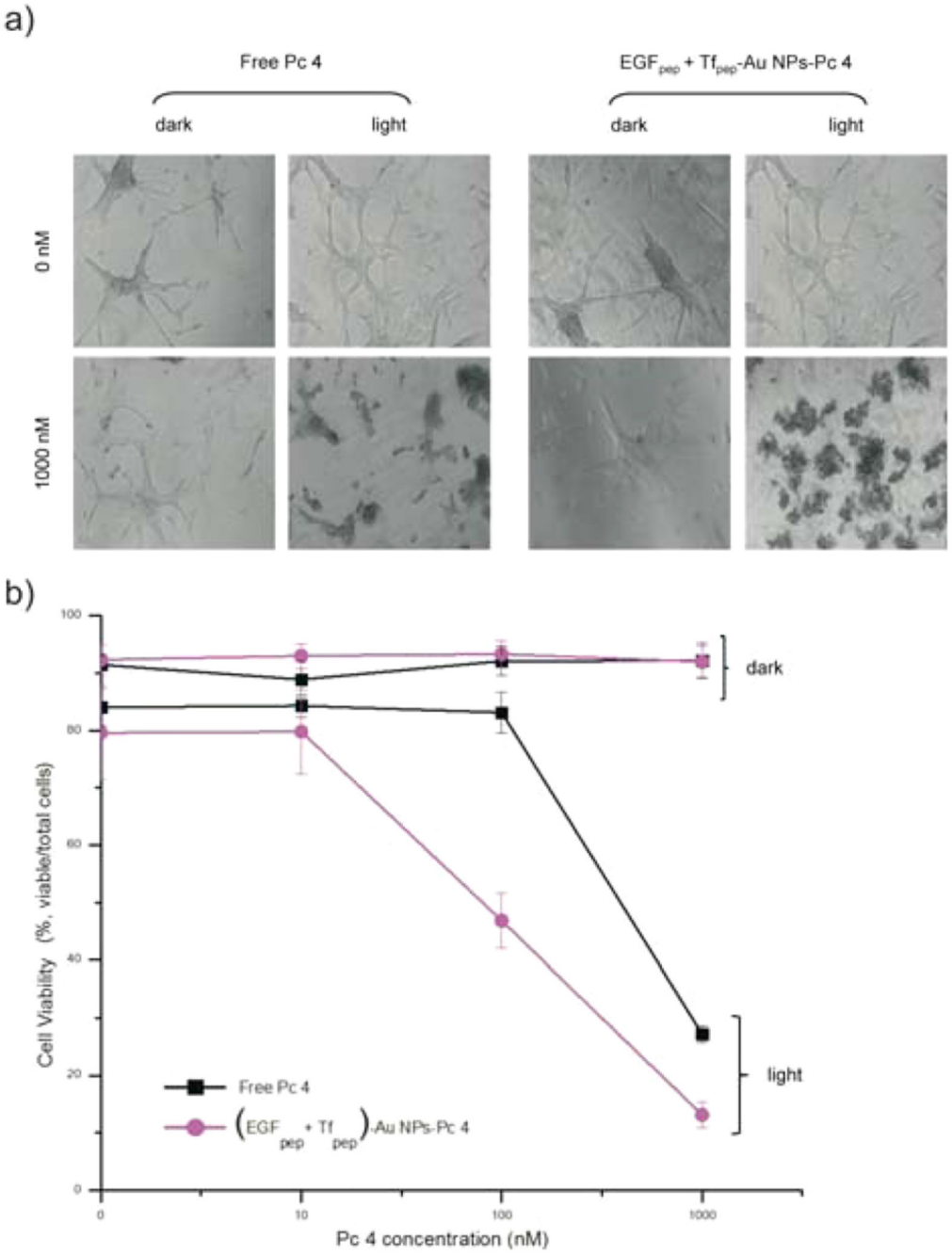

Figure 5.

Dual targeted AuNPs efficacy in killing U87 cells. (a) Cell morphology of U87 cells treated with 500 nM of (EGF_{pep}+Tf_{pep})-AuNPs-Pc 4 versus standard of care free Pc 4 at 0 or 1000 nM Pc 4 for 4 h and either unactivated (dark) or activated (light) by light (670 nm, 0.83 J cm^{-2} s^{-1}). (b) Cell viability was quantified after 4 h using flow cytometry.

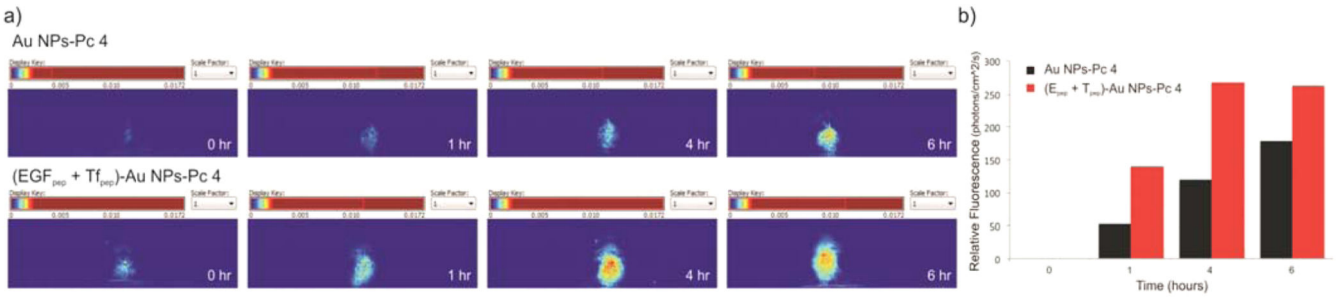

Figure 6.

Pc 4-loaded dual-targeted AuNPs for differential *in vivo* detection of tumors. (a) Representative normalized (hotmap) images of fluorescence reconstruction showing the targeting of (EGF_{pep}+Tf_{pep})-AuNPs-Pc 4 versus untargeted AuNPs-Pc 4 to orthotopic brain tumors after 1, 4, and 6 h post injection. (b) Graph of average Pc 4 fluorescence intensity signal in mice bearing orthotopic U87 tumors with (EGF_{pep}+Tf_{pep})-AuNPs-Pc 4 or AuNPs-Pc 4.